The ebb and flow of protons: A novel approach for the assessment of estuarine and coastal acidification

D.T. Pettay[*†‡], S.F. Gonski[§,¶], W.J. Cai[§], C.K. Sommerfield[†], W.J. Ullman[†]*

[†]School of Marine Science and Policy, University of Delaware, Lewes, DE, USA

‡Department of Natural Sciences, University of South Carolina Beaufort, Beaufort, SC USA

[§]Washington State Department of Ecology, Olympia, WA, USA

[§]School of Marine Science and Policy, University of Delaware Newark, DE, USA

ABSTRACT:

The acidification of coastal waters is a consequence of both natural (e.g., aerobic respiration) and anthropogenic (e.g., combustion of fossil fuels, eutrophication) processes and can negatively impact the surrounding ecosystems. Until recently it was difficult to accurately measure estuarine pH, and thus total proton concentrations ($[H_T^+]$), when salinities vary significantly and rapidly as a consequence of tidal mixing. Proton production and transport are ultimately responsible for acidification in coastal environments, and the uncertainty surrounding proton concentrations measured at high frequency has hindered our understanding of the net impact of global and local processes on estuarine acidification. Here, we quantify the rate of proton exchange between an estuary and bay to assess the extent of acidification by using the novel combination of high frequency pH_T (total hydrogen ion concentration scale) data from an autonomous SeapHOx^{TM} sensor and continuous tidal discharge measurements made between the eutrophic Murderkill Estuary and Delaware Bay. Proton fluxes reverse with each tide. However,

the net non-tidal proton fluxes are directed upstream and display seasonal changes in magnitude. Our results indicate that Delaware Bay contributes to the acidification of the Murderkill Estuary, yet the degree of acidification is reduced in the summer. Using proton concentrations measured at high temporal resolution to calculate proton fluxes provides a new and relatively simple approach for quantifying the acidification of dynamic nearshore environments.

Keywords: Coastal acidification, Proton concentrations, Fluxes, pH, Continuous monitoring, Delaware Bay, Murderkill River

1. INTRODUCTION:

Acidification of natural waters represents a net increase in hydrogen ion concentration ([H^+] or "protons") that is dependent on changes in the magnitude of proton-producing and -consuming processes (Hoffman *et al.* 2009). Open-ocean acidification, due primarily to the dissolution of atmospheric CO_2 into seawater to produce carbonic acid (H_2CO_3), progresses at relatively the same rate around the world (-0.001-0.002 pH units/year), while the rates in estuaries and the coastal ocean are consistently estimated to be an order of magnitude higher (Provost *et al.* 2010, Duarte *et al.* 2013, Carstensen and Duarte 2019). In estuarine and coastal waters CO_2 dissolution combines with local eutrophication and the aerobic respiration of allochthonous and autochthonous organic matter to enhance acidification (Sunda & Cai 2012, Wallace *et al.* 2014). As the delivery of nutrients and organic carbon to estuaries and coastal waters increase, higher rates of local acidification are anticipated (Feely *et al.* 2010, Cai *et al.* 2011, Wallace *et al.* 2014). Conversely, biological processes like primary production and mineral dissolution moderate acidification by consuming CO_2 (Borges & Gypens 2010; Aufdenkampe *et al.* 2011, Duarte *et al.* 2013). Due to the large number of competing acid-consuming and -producing processes and environmental proton sources and sinks, it is challenging to determine the net rates of all of processes that contribute to and mitigate the acidification of any particular water body (Hofmann *et al.* 2010 and the references therein).

Proton cycling is the sum of all proton-consuming and -producing processes within a body of water. In an estuary this cycling is influenced by a number of hydrophysical and hydrochemical processes. In general, proton concentrations are elevated (lower pH; pH = $-log[H_T^+]$) in the upper watershed and around marshes due to freshwater inputs, respiration and nitrification. These elevated concentrations flow downstream on the ebb tide and into the

52 nearshore coastal waters where protons are consumed by primary production and CO_2 degassing
53 and, together with dilution and carbonate buffering, cause proton concentrations in the waters of
54 the returning flood tide to decline (pH increases; Cai *et al.* 2000, Wang & Cai 2004, Hofmann *et*
55 *al.* 2009).

56 The imbalance between proton sources and sinks explicitly leads to long-term changes in
57 acidity and is highly variable among coastal systems. This fact is leading to a transition away
58 from a pH-dependent examination of estuarine and ocean acidification, and towards the inclusion
59 and analyses of proton concentrations (Hofmann *et al.* 2010, Fassbender *et al*. 2017,
60 Kwiatkowski & Orr 2018). Therefore, the determination of proton production, consumption, and
61 transport is needed to assess: (1) whether a particular water body will become acidified; (2) the
62 rate and extent of acid production and consumption within the water body; and (3) the rates and
63 direction of proton exchange between adjacent and connected water bodies. Measured proton
64 fluxes can help address this need by quantifying the rates of proton cycling and acidification
65 within coastal waters. Changes in carbonate chemistry (dissolved inorganic carbon; DIC and
66 total alkalinity; TA) are commonly used to calculate pH and to determine the rates of
67 biogeochemical processes leading to the acidification of natural waters, however, this approach
68 is time consuming, tedious, and rarely capable of producing pH measurements over the temporal
69 and spatial scales that approximate the inherent variability of physically and biogeochemically
70 dynamic coastal waters (see Section 3.1 for further discussion; Hofmann *et al.* 2008, Hofmann *et*
71 *al.* 2010). Recent advances in pH sensor technology bridge this gap and now provide the
72 opportunity to calculate the flux of protons between water bodies, an innovative approach to
73 assess acidification.

74 To date, we are aware of only one estuarine system for which the notion of proton
75 cycling has been considered, the Scheldt Estuary, where the net consumption of protons
76 (modeled at 20 kmol y^{-1} for the whole estuary) has already resulted in a gradual increase in
77 estuarine surface pH over time (Borges & Gypens 2010, Hofmann *et al.* 2009). While proton
78 fluxes have been discussed in coral reef systems and analyzed on a global scale relative to
79 changes in pCO_2 (e.g., Jokiel 2016, Fassbender *et al*. 2017), similar quantification of net proton
80 fluxes within and between estuarine water bodies, as was done in the Scheldt, is not available.
81 However, quantification of these fluxes can help determine the ultimate impact of acidification
82 on ecosystems and ecological processes, and to develop practical and scalable mitigation
83 strategies for acidification-dependent environmental degradation. Here we report measured
84 proton concentrations and calculated fluxes within a dynamic estuarine environment (the
85 confluence of eutrophic Murderkill Estuary and Delaware Bay, Delaware, USA; Fig. 1).
86 Instantaneous fluxes were determined for the biologically productive Spring and Summer
87 months in 2016, using high frequency pH data from a SeapHOx ™ sensor and discharge
88 measurements at a US Geological Survey (USGS) gaging station. Agricultural runoff and
89 discharge from a wastewater treatment plant significantly influence estuarine water quality
90 within the Murderkill Estuary. As a consequence of these inputs, (1) nutrient concentrations are
91 elevated in the upper Murderkill Estuary; (2) the estuary experiences hypoxia during the summer
92 months; and (3) nitrogen and phosphorus burial rates in the adjacent marsh sediments have
93 increased two-fold since the mid-1970s (Velinsky *et al.* 2010). As such, this eutrophic estuary
94 makes an ideal case study to quantify the influence of proton cycling and exchange on the coastal
95 ocean.
96

2. MATERIALS AND METHODS:

2.1 Site Description

The Murderkill Watershed and Estuary are located in southeastern Kent County, Delaware (Fig 1). The 342 km^2 watershed is predominantly agricultural (56%), with lower fractions of urban (16%), forested (11%), and wetlands (including forested wetlands, 17%) land-uses (Ullman *et al.* 2013). The watershed has well-drained soils, consistent with its coastal plain setting (Andres 2004). Most of the rural development in the watershed disposes of its wastewater through domestic septic and small community systems (DNREC 2006). However, the Kent County Regional Resource Recovery Facility (KCRRRF) that discharges to the upper Murderkill Estuary treats wastewater originating from both within and outside the watershed, including the nearby urban centers of Dover, Smyrna, and Milford, Delaware (Fig. 1). Discharge from the KCRRRF increases the effective anthropogenic pressure on the Estuary and its downstream waters. The Murderkill Estuary has an average width of 50 m and an average channel depth of 4.5 m, and discharges to Delaware Bay at Bowers, Delaware, approximately 39 km upstream of the Delaware Bay mouth, where it supports high and persistent levels of primary production in the Bay margins during the summer months (Wong *et al.* 2009, Voynova *et al.* 2015). The Delaware Bay drains a 36,570 km^2 watershed that encompasses parts of Delaware, New Jersey, Pennsylvania, and New York State with the tidal portion extending 215 km into New Jersey and Pennsylvania (Voynova *et al.* 2015). The width of the Bay increases from about 18 km at the mouth to about 44 km upstream and has a mean depth of 6 m (Sharp *et al.* 2009, Wong *et al.* 2009). The Delaware and the Schuylkill Rivers provide more than 70% of the freshwater flow into the Bay, but numerous small tributaries, including the Murderkill River, discharge along the margins of the bay and contribute significant nutrient loads into the Bay (Voynova and Sharp

2012, Voynova *et al.* 2015). Discharge through the River/Bay is typically higher in the Spring than the summer, however, in 2016 the Spring was drier than the Summer by ~30 mm in precipitation for the Murderkill Estuary (data from Kitts Hummock National Estuarine Research Reserve (NERR) station <nerrsdata.org/get/realTime.cfm?stationCode 1/4 DELSJMET>; approximately 5 km northwest of Bowers). Temperature, salinity and pH are temporally and tidally variable in both the Murderkill River and the Delaware Bay, with ranges for the River/Bay system of ~0 - 33°C, 3 - 30 g/kg and 6.5 - 8.3, respectively (Ullman *et al.* 2013, Voynova *et al.* 2015, Gonski *et al.* 2018).

2.2 Instrumentation

The SeapHOx sensor package is integrated with sensors for temperature, salinity (Sea-Bird Electronics Conductivity-Temperature Sensor – SBE37), pH (Honeywell Durafet), and oxygen (Aanderaa Data Instruments 4835 Optode) deploying in sequence as water is pumped through the sensor flow path by a Sea-Bird Electronics 5M submersible pump (Bresnahan *et al.*, 2014). The SeapHOx was deployed at the confluence of the Murderkill Estuary and Delaware Bay where it sampled waters discharging from the Estuary to the Bay on falling tides and waters recharging the Estuary from the Bay on rising tides. The SeapHOx was deployed adjacent to the main tidal channel of the Estuary at approximately 1 m above the estuarine floor and 3 m below mean high tide. During the Spring (12 May to 09 June) and Summer (20 July to 24 August) 2016 the sensor measured pH_T, temperature, and salinity every 30 minutes. Due to sedimentation and biofouling, the instrument was cleaned and serviced at intervals of 1-2 weeks and data were not collected during the servicing periods when the instrument was out of the water (described by Gonski *et al.* 2018). The US Geological Survey operates a tidal gauging station at this site

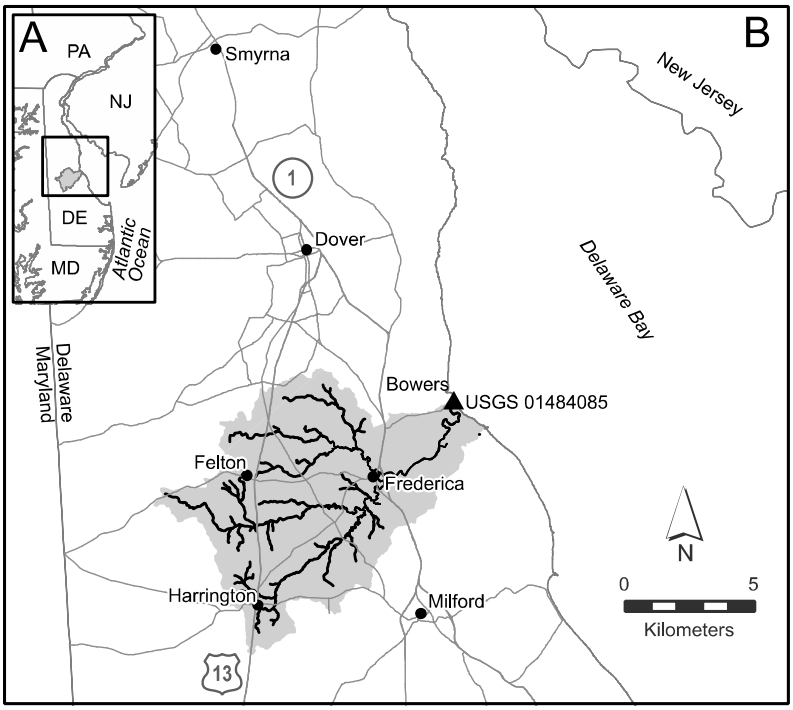

Fig. 1. Map of the Murderkill Watershed and sensor location. Location of the Murderkill Watershed in the Mid-Atlantic and state of Delaware (A, inset). The Murderkill Watershed (grey) and the USGS gauging station (DE01484085) in Bowers, Delaware (triangle) at the confluence of the Murderkill Estuary and Delaware Bay (B). An autonomous pH sensor was co-located at the USGS gauging station during the Spring and Summer of 2016.

149 (USGS 01484085), in cooperation with the Delaware Geological Survey and the State of
150 Delaware. Consistent with the USGS convention, positive discharges and fluxes are directed
151 downstream. Co-located with these instruments was a Seabird Scientific Land Ocean
152 Biogeochemical Observatory that provides additional biogeochemical data (not reported here)
153 for both the Murderkill Estuary and from Delaware Bay depending on the direction of tidal flows
154 (Voynova *et al.*, 2015).

155 *2.3 SeapHOx Calibration*

156 The Honeywell Durafet and its integrated reference electrodes, built into the SeapHOx
157 sensor, calculate and report a pair of pH values on the total scale (pH_T): pH^{INT} (internal
158 reference, Ag/AgCl reference electrode containing a 4.5 KCl gel liquid junction, FET|INT) and
159 pH^{EXT} (external reference, solid-state chloride ion-selective electrode, Cl-ISE, FET|EXT). The
160 SeapHOx was calibrated using an *in situ* or field calibration procedure where discrete bottle
161 samples were collected in the field for laboratory analysis of DIC and TA alongside
162 simultaneous SeapHOx sensor measurements. Duplicate bottle samples were collected for DIC
163 and TA analysis in triple-rinsed 250-mL borosilicate glass bottles by bottom-filling and
164 overflowing following filtration through Whatman 0.45 mm Polyethersulfone (PES) filters (GE
165 Healthcare Bio-Sciences, Pittsburgh, PA, USA). The calibration samples were fixed with 100 µL
166 of saturated mercuric chloride ($HgCl_2$), securely closed, and stored on ice and in the dark at ~4°C
167 until returned to the laboratory for analysis (Cai and Wang 1998; Huang *et al*. 2012). Calibration
168 samples for the Spring (N = 21) and Summer (N = 24) pH time-series were collected every 30
169 minutes on 01 June 2016 and 02 August 2016, respectively, over full tidal cycles to capture the
170 entire salinity range observed on those days (Gonski *et al.* 2018). DIC was determined in the
171 laboratory, as CO_2 gas, using a non-dispersive infrared gas analyzer (AS-C3 Apollo SciTech)

following sample acidification. TA was determined by Gran Titration (Gran 1950, 1952) using a semi-automated open-cell titration system (AS-ALK2 Apollo SciTech) (Cai *et al.* 2010; Huang *et al.* 2012; Wang and Cai, 2004). Both instruments were calibrated using certified reference materials (CRMs), provided by A.G. Dickson (Scripps Institution of Oceanography), yielding results with a precision of ±2.2 μmol kg^{-1}. A set of reference pH measurements for the calibration samples was calculated on the total scale from measured DIC and TA at *in situ* temperature, salinity, and pressure using the inorganic carbon dissociation constants of Millero *et al.* (2006), the bisulfate ion acidity constant of Dickson (1990), and the boron-to-chlorinity ratio of Lee *et al.* (2010) using the Excel macro CO2SYS (Pierrot *et al.* 2006). The sensor data was then recalibrated to minimize the anomaly between the sensor pH_T and reference pH_T determined from the calibration samples by setting the calibration constants specific to each reference electrode to average values based on all valid calibration samples (Bresnahan *et al.* 2014).

Using this rigorous calibration scheme, the sensor pH had root-mean-square errors of 0.0275 and 0.0159 pH units for the Spring and Summer periods, respectively, relative to pH_T calculated from measured DIC and TA (Gonski *et al.* 2018). The pH_T and salinity of calibration samples on 1 June 2016 ranged between 7.1 and 8.3 and 8.99 and 22.31, respectively. On 2 August 2016, pH_T and salinity of calibration samples ranged between 7.0 and 7.9 and 21.07 and 27.06, respectively. In the present work, the pH^{INT} time-series was used for both time periods as pH measured with the internal reference electrode and calibrated using an *in situ* multi-point calibration approach, which provides a more robust measurement over a wide range of time-varying salinities in nearshore estuarine environments (Gonski *et al.* 2018; Miller *et al.* 2018).

194 For a more thorough discussion of the sampling approach and sensor calibration, the reader is
195 referred to Gonski *et al.* (2018).

196 No corrections were made for possible "excess" (non-carbonate) alkalinity in the
197 calibration samples. This contribution to alkalinity is not likely to exceed 1-2% of the total
198 alkalinity and therefore should have no significant impact on the SeapHOx calibration (Gonski *et*
199 *al.* 2018). The present pH data closely approximates the precision recommended by the Global
200 Ocean Acidification Observing Network (GOA-ON) for weather-level pH measurement
201 precision (Newton *et al.*, 2015), and, as such, are sufficient for resolving the directions and
202 magnitudes of proton fluxes between the Murderkill Estuary and Delaware Bay.

203 *2.4 Time Series Analysis*

204 Prior to flux calculations, the half-hourly measured continuous pH_T data was interpolated
205 linearly to match the six-minute interval of the discharge measurements. Instantaneous proton
206 concentrations on the total hydrogen ion concentration scale were calculated from the measured
207 values of pH_T and the definition of pH_T:

208 $$[H_T^+] = 10\text{^}(-pH_T)$$

209 The non-tidal component was separated from the instantaneous time series for discharge
210 and $[H_T^+]$ using a 40-hour low-pass Butterworth filter (Ganju *et al.* 2005, Dzwonkowski et al.
211 2014). Filtering was performed in R using the 'signal' package (Ligges *et al.* 2013) with a
212 double-pass filter and n=3 (i.e., 3rd order), removing all variation due to tidal harmonics. The
213 filtered non-tidal discharge and $[H_T^+]$ were used to calculate net non-tidal fluxes for each
214 sampling period. The instantaneous data for salinity was also linearly interpolated and filtered as
215 described above to calculate a salt flux for each period. Salinity represents a conservative

constituent and was used to validate the flux calculations. For the purposes of calculating fluxes, salinity was considered to be in units of g kg^{-1}.

2.5 Subsampling of Protons

High frequency, continuous monitoring reveals patterns in biogeochemical processes that may be missed using less frequent, single time point sampling typical of historical sampling strategies. To further demonstrate this point we randomly subsampled interpolated proton concentrations from the Spring and compared the distribution of the means of these subsamplings to that of the overall mean. Four hypothetical "sampling" strategies were developed and consisted of random pH measurements taken during three-hour windows (similar to recommended by Skeffington *et al.* 2015) either in the morning (9:00 to 11:00) or afternoon (14:00 to 16:00) and sampled every other day starting either on day 1 or day 2 of the Spring dataset. These four subsamplings were therefore named day1AM or day1PM, and day2AM or day2PM. A proton concentration was randomly drawn in the morning or afternoon on every other day and a mean was computed from all of these single daily measurements. Each subsampling was repeated 10,000 times and the frequency distributions of the means were plotted against each other and the overall mean for the Spring 2016.

2.6 Flux Calculations

Advective fluxes of dissolved material C (J_C) can be calculated as the product of concentration (C, mass/m^3) and discharge (Q, m^3/time) for any period for which instantaneous or integrated C and Q are both available or can be estimated:

$$J_c = (C \times Q)$$

237 The instantaneous density of seawater, determined using salinity and temperature, was used to
238 convert kg to m^3. In this study, net non-tidal fluxes of proton and salt concentrations were
239 calculated using the low-pass filtered data for both C and Q. The mean and standard error of the
240 fluxes (Table 1) were calculated for seasonal discharge measurements and flux calculations.

241 **3. RESULTS AND DISCUSSION:**

242 *3.1 Measuring protons in dynamic saline environments: Why now?*

243 Previous work has criticized the strong focus on alkalinity changes when characterizing
244 the acid-base chemistry of natural waters (Hofmann *et al.* 2010), while others have further
245 discussed the limitations of using pH to assess acidification, showing proton concentrations to be
246 a more robust indicator (Fassbender *et al*. 2017, Kwiatkowski & Orr 2018). Changes in observed
247 pH actually reflect proton consumption and production by numerous biogeochemical processes,
248 and only indirectly involve alkalinity reactions (Hofmann *et al.* 2010). These processes are
249 seasonal in nature and geographically variable, and using pH to quantify acidification captures
250 only a small portion of this variability when compared to $[H_T^+]$ (Fassbender *et al*. 2017,
251 Fassbender *et al*. 2018a & b, Kwiatkowski & Orr 2018). In fact, across most latitudes seasonal
252 pH variability is projected to decrease in the future, while proton variability is predicted to
253 significantly increase (Fassbender *et al*. 2017, Kwiatkowski & Orr 2018). The differences
254 between these two seemly identical measurements are due to the logarithmic nature of the pH
255 scale and the complexity of the carbonate buffering in salt water. These modeling efforts are
256 extremely informative on a global and regional scale, however, they do not explicitly account for
257 or document the high frequency temporal variations that occur within individual coastal systems
258 (Fig. 2). As such, there is a strong need for high frequency, long-term measurements of $[H_T^+]$
259 across distinct coastal and estuarine systems to better understand shorter-term variability and

seasonal differences so that this information can be incorporated into predictive models (Fassbender *et al*. 2018).

Cation interferences on the performance of *in situ* glass electrodes, together with their slow response time, previously made continuous measurements of pH in estuaries with rapidly varying salinity highly uncertain. This traditional methodology of using glass electrode potentiometry to yield proton activities is subject to unpredictable and irreproducible liquid junction errors in brackish and saline waters (Bates 1973, Butler *et al.* 1985, Easley & Byrne 2012, Whitfield *et al.* 1985), often making the conversion of proton activity to proton concentration imprecise (Dickson 1984). Accordingly, glass electrode potentiometry is no longer the preferred methodology in contemporary studies of pH in marine and estuarine waters, unless used with alternative methods of calibration (Easley & Byrne 2012; Wootton & Pfister 2012; Martz *et al*. 2015; Gonski *et al.* 2018). In seawater, the determination of proton concentrations on the total hydrogen ion concentration scale (pH_T) is now preferred (Dickson 1984, 1993).

To overcome the above analytical issues, several autonomous biogeochemical sensors built around a proton-sensitive Ion-Selective Field-Effect Transistor (ISFET) were developed to yield more rapid, precise, accurate, and reproducible pH_T measurements in natural waters, including seawater (Bresnahan *et al.* 2014; Martz *et al.* 2010). When used with appropriate calibration procedures, these ISFETs are subject to substantially less interference from seawater cations, have smaller "memory" effects, improved long-term stability and responds more rapidly than the glass electrode to changes in ambient proton concentrations in estuarine and marine settings (Martz *et al.* 2010, Bresnahan *et al.* 2014, Takeshita *et al.* 2014, Gonski *et al.* 2018). Using this recent advance in pH sensor technology, together with appropriate sensor deployment and calibration procedures (Bresnahan *et al.* 2014, Gonski *et al.* 2018, Miller *et al.* 2018), $[H_T^+]$

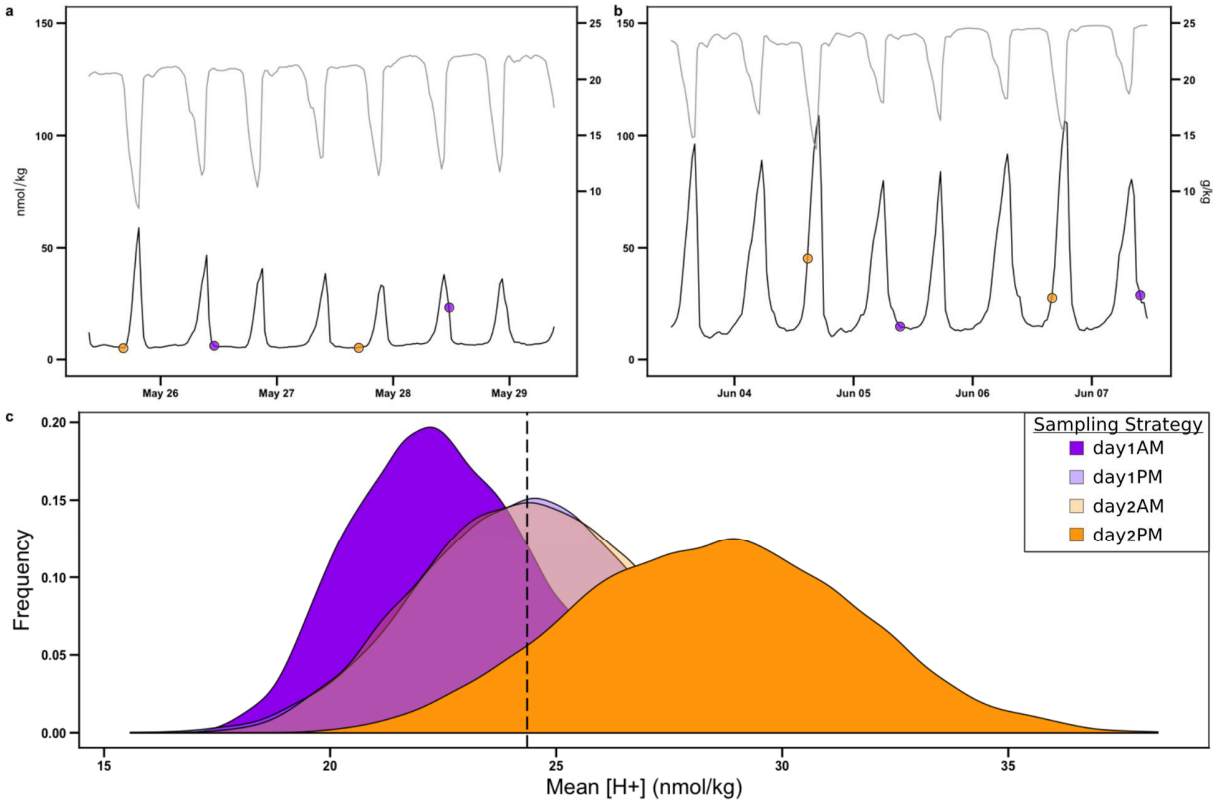

Fig. 2. A conceptualization of short-term variability in proton concentrations due to tidal forcing based on data collected in Spring 2016. Proton concentrations (black) for both neap (a) and spring (b) tides. Salinity (grey) is plotted as a surrogate for tidal stage, where salinity maxima occur during flood tides and minima occur during slack ebb tides. Colored points (a & b) are examples of randomly sampled time points for day1AM and day2PM only (see Methods for description of subsampling). These points demonstrate real variability missed when sampling at lower frequencies and how different sampling strategies can lead to differing values of mean proton concentration. Frequency distributions of mean proton concentrations based on four subsampling schemes (c); day1AM (purple), day1PM (light purple), day2AM (light orange), day2PM (orange), and the overall mean for Spring 2016 (dashed line). Day1PM and day2AM distributions overlap each other and the overall mean for the Spring.

296 (nmol kg^{-1}) and fluxes (mmol h^{-1}) within and between physically dynamic estuarine and marine
297 environments can now be reliably determined with high temporal resolution and in the same
298 manner as the fluxes of other dissolved constituents (for an illustrated demonstration of flux
299 calculation see Fig. 3).

300 The combination of tidal forcing and biogeochemical processes with respect to sampling
301 date and time can both influence measured $[H_T^+]$ and our understanding of proton dynamics
302 (Hofmann *et al.* 2009, Ullman *et al.* 2013). A conceptualization of the short-term variability in
303 $[H_T^+]$ due to tidal forcing and its influence on conclusions drawn from lower frequency sampling
304 is shown in Fig. 2. Proton concentrations from the Spring dataset were randomly sampled, means
305 computed and the frequency distribution of 10,000 iterations plotted against the overall mean for
306 the Spring (see Methods). An example of this random sampling shows that the extent to which
307 $[H_T^+]$ variability due to tidal forcing is missed with less frequent samplings (Fig. 2a & b, orange
308 and purple points). The frequency distributions show, even in this simple example, that sampling
309 strategy can significantly affect the mean of measured $[H_T^+]$ and highlight the need for high
310 frequency monitoring to truly understand acidification in these dynamic systems (Fig. 2c).
311 Similar and more in-depth comparisons of the sample frequency for water quality monitoring
312 show similar patterns (Skeffington *et al.* 2015, Gonski *et al.* 2018, Chappell *et al.* 2017, Miller *et*
313 *al.* 2018). However, our subsampling does show that prior knowledge of the high frequency
314 dynamics of $[H_T^+]$ over time might allow for a lower frequency sampling strategy that
315 approximates the means obtained from higher frequency monitoring (Fig. 2c).

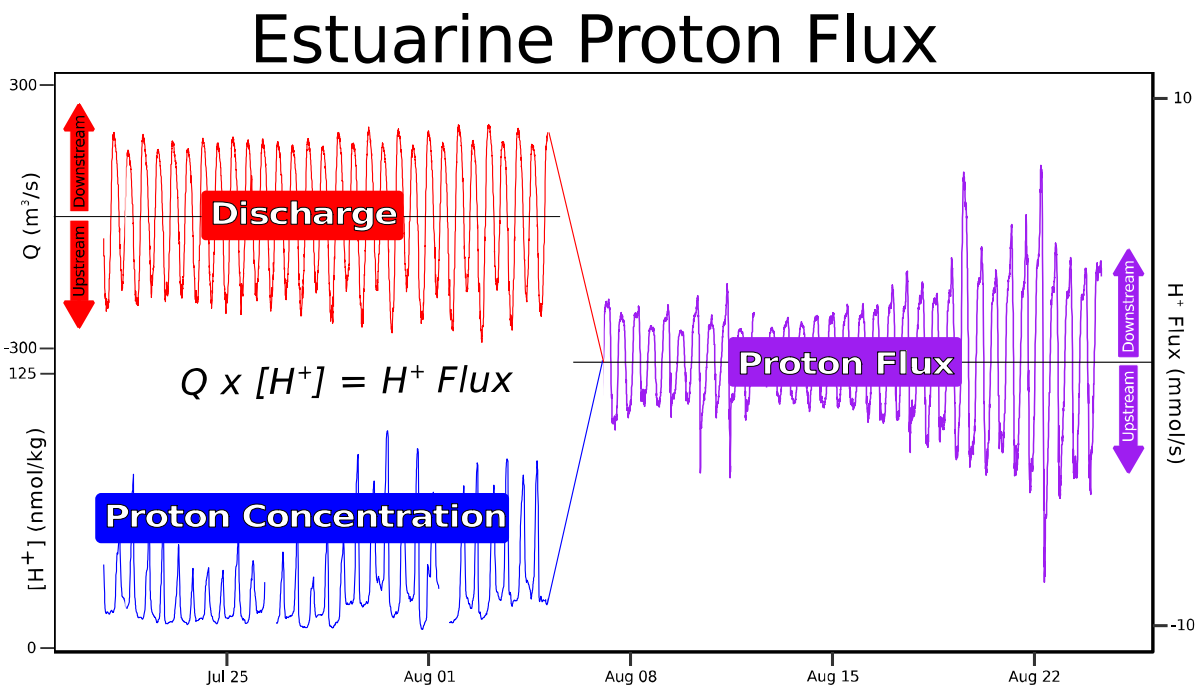

316

317 **Fig. 3.** Illustration of flux calculations using the product of discharge (Q, red) and proton
318 concentration ($[H_T^+]$, blue) to determine instantaneous proton fluxes (H^+ Flux, purple). Positive
319 values for discharge and flux indicate downstream flow, with negative values indicating
320 upstream flow. Note that this illustration depicts an unfiltered flux to demonstrate the influence
321 of tidal harmonics. The seasonal fluxes reported in this paper are filtered to remove these
322 influences.

323 *3.2 Proton Fluxes through the Murderkill*

324 Mean non-tidal proton fluxes were calculated for the two seasonal periods using time
325 series of low-pass filtered, instantaneous proton concentration and discharge measured at the
326 mouth of the Murderkill River. We use the term "non-tidal" because filtering removes the
327 influence of tidal variability and represents the net flux of protons upstream or downstream (see
328 Methods). Instantaneous non-tidal proton fluxes ranged from -0.71 to 1.4 mmol h^{-1} in the Spring,
329 and from -0.57 to 0.6 mmol h^{-1} in the Summer (Figs. 4 & 5), where positive flow is downstream.
330 As a result, the Estuary's average upstream proton flux decreased by over 7-fold from the Spring
331 (-9.6 ± 5.5 mmol h^{-1}) to the Summer (-1.3 ± 2.8 mmol h^{-1}; Table 1). A portion of this seasonal
332 decrease is likely related to changes in non-tidal discharge during a drier Spring 2016 (total
333 precipitation to the Murderkill was ~30 mm lower, data not shown), leading to less freshwater
334 and proton input into the Estuary and a larger upstream discharge due to tidal forcing (Table 1).
335 In addition to discharge, changes in the magnitude of proton-producing processes like respiration
336 and nitrification, and proton-consuming processes like primary production and CO_2 degassing
337 will also influence proton cycling and the flux of protons (Cai *et al.* 2000, Wang & Cai 2004,
338 Hofmann *et al.* 2009).

339 The proton fluxes calculated here correspond surprisingly well with those modeled by
340 Hofmann *et al.* for the Scheldt Estuary (2009). Although the Scheldt is much larger than the
341 Murderkill Estuary and differs in its history and magnitude of human impacts, both systems are
342 temperate, coastal plain estuaries that are turbid and nutrient-rich, and contain extensive salt
343 marshes and mudflats (De Vriend et al. 2001, Ullman *et al.* 2013). While Hofmann and
344 colleagues modeled *in situ* proton production and consumption, as opposed to the proton fluxes,

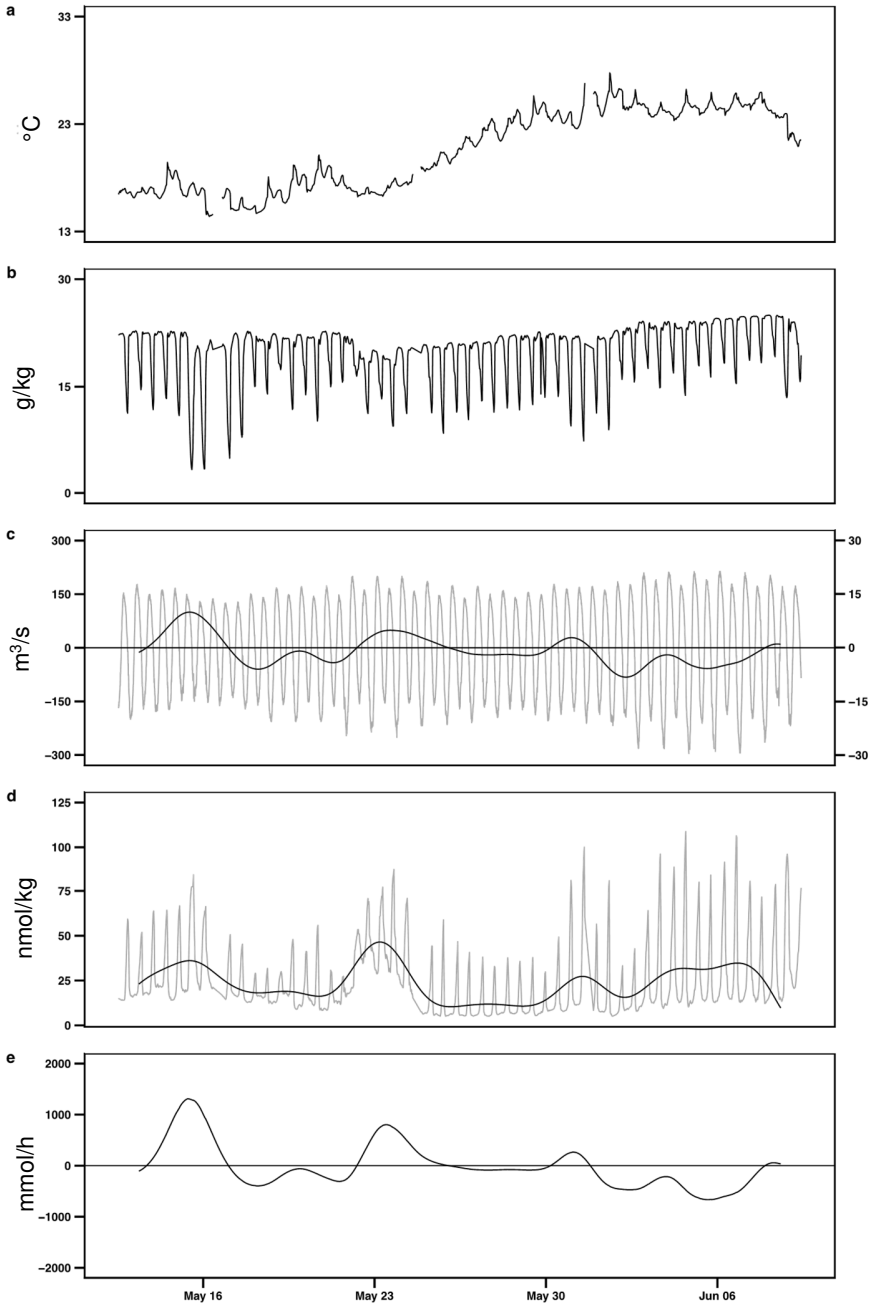

345 **Fig. 4.** Raw and filtered time series data between the Murderkill Estuary and Delaware Bay at
346 Bowers Delaware during Spring of 2016. Time series of (a) temperature, (b) salinity, (c)
347 discharge, (d) proton concentrations and (e) proton fluxes. Both the original data (grey line in c
348 & d) and the non-tidal components (black line in c & d) of the original data, filtered using a low-
349 pass Butterworth filter, are shown for discharge and protons. Proton fluxes were calculated from
350 the non-tidal component of discharge and protons. Positive discharges and fluxes are directed
351 downstream toward Delaware Bay.

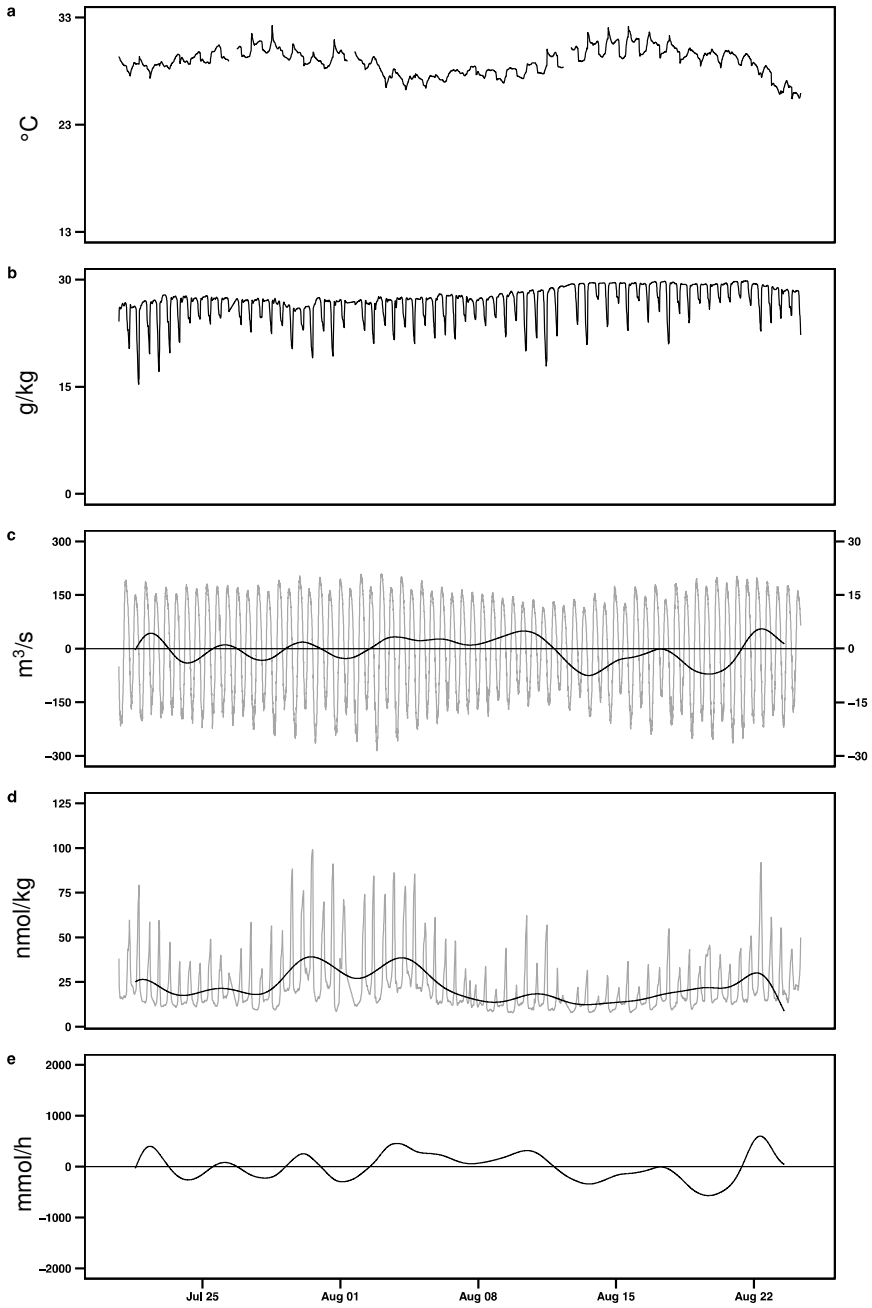

Fig. 5. Raw and filtered time series data between the Murderkill Estuary and Delaware Bay at Bowers Delaware during Summer of 2016. Time series of (a) temperature, (b) salinity, (c) discharge, (d) proton concentrations and (e) proton fluxes. Both the original data (grey line in c & d) and the non-tidal components (black line in c & d) of the original data, filtered using a low-pass Butterworth filter, are shown for discharge and protons. Proton fluxes were calculated from the non-tidal component of discharge and protons. Positive discharges and fluxes are directed downstream toward Delaware Bay.

359 the results are comparable. Summing the yearly consumption/production rates across their
360 modeled boxes yields a net consumption of protons (increase in pH_T) that ranged from -0.03
361 kmol yr^{-1} ~100km upstream to -0.40 kmol yr^{-1} at the mouth. Extrapolating our hourly fluxes to
362 yearly gives a range of -0.08 kmol yr^{-1} to -0.01 kmol yr^{-1} using 12 months of either Spring or
363 Summer rates, respectively. This annual flux is only an order of magnitude lower than that
364 calculated for the mouth of the Scheldt Estuary, despite the Murderkill watershed being
365 approximately two orders of magnitude smaller. Additional analyses over an entire year are
366 clearly needed to provide a true annual flux for the Murderkill Estuary; however, it is
367 encouraging that our calculated fluxes align with modeled values for another eutrophic, coastal
368 plain estuary.

369 Our flux calculations demonstrate that the Murderkill Estuary transports protons
370 downstream and contributes to the acidification of Delaware Bay, but only for short periods of
371 time (hours to days). Over longer periods, the Estuary acts as a sink for protons coming from the
372 Bay and coastal ocean, likely driven by alkalinity generated during anaerobic respiration in
373 marsh sediments (Ullman *et al.* 2013, Wang & Cai 2004). The Murderkill Estuary discharges ~
374 39 km upstream of the Bay's mouth and lies within a region where pH is highest for the Bay
375 (Joesoef *et al.* 2017). Nutrient transport down the Murderkill stimulates phytoplankton
376 productivity in the Bay (Voynova *et al.* 2015), thus reducing DIC and elevating pH. Other rivers
377 discharge within this region too (including the St. Jones, Mispillion Rivers and Cedar Creek in
378 Delaware and the Maurice River in New Jersey), and may all contribute to the observed spike in
379 pH. Similar to proton flux, the pH within the Bay shows seasonal variation related to
380 meteorological events and biogeochemical processes within the watershed (Joesoef *et al.* 2017).
381 If freshwater discharge has the largest impact on the long-term trend of $[H_T^+]$ in the Murderkill

382

Table 1: Summary of mean Spring and Summer fluxes from the Murderkill Estuary to Delaware Bay in 2016 (± standard error).

Non-Tidal Flux*	Spring 2016	Summer 2016
Water	-0.78 ± 0.05 m^3/s	-0.40 ± 0.04 m^3/s
Salt	-75 ± 3.5 Mg/h	-48 ± 3.7 Mg/h
Protons	-9.6 ± 5.5 mmol/h	-1.3 ± 2.8 mmol/h

383 * Positive fluxes are directed downstream towards the Bay.

384 (e.g., Hofmann *et al.* 2009), it will be interesting to see how proton fluxes change over the
385 course of a year and if the Estuary is truly a net sink for protons. These analyses will reveal the
386 buffering effect of the Murderkill Estuary, along with other nearby estuaries, on Delaware Bay
387 and the coastal ocean.

388 *3.3 Tidal and Seasonal Changes in Proton Concentrations*

389 Daily and seasonal variations in the pH of estuaries, bays and coastal oceans have been
390 fairly well documented (e.g., Wang & Cai 2004, Hofmann *et al.* 2011, Kline *et al.* 2015, Rivest
391 & Gouhier 2015, Takeshita *et al.* 2015, Wang *et al.* 2016), including the Delaware Bay (Joesoef
392 *et al.* 2017, Gonski *et al.* 2018). Proton concentrations at the mouth of the Murderkill River
393 tracks tidal advection and, therefore, is inversely related to tidal cycle and salinity (Fig. 2a & b).
394 The lowest $[H_T^+]$ (highest pH_T) occur during flood tides when saline Delaware Bay water flows
395 into the lower Murderkill Estuary. As the tide ebbs, $[H_T^+]$ increases (pH_T decreases) and reaches a
396 maximum during the slack-low tide. In contrast to the flood tide, which produces a prolonged
397 minimum in $[H_T^+]$, concentrations peak for only a short period of time (typically less than an
398 hour) at slack ebb tide.

399 Respiration (a proton source) and primary production (a proton sink) are tidally coupled
400 between the Murderkill Estuary and Delaware Bay, and contribute to the patterns described
401 above (Voynova *et al.* 2015). Nutrients and DIC are transferred downstream and fuel primary
402 productivity, the products of which (reactive organic matter) are subsequently transferred back
403 upstream and fuel respiration (Wang & Cai 2004, Voynova *et al.* 2015). Therefore, lower salinity
404 waters discharging from the Murderkill Watershed (and to a lesser extent the wastewater
405 treatment plant) are characterized by higher turbidity, undersaturated levels of dissolved O_2 and
406 elevated DIC associated with net respiration and the production of protons (Ullman *et al.* 2013,

407 Voynova *et al.* 2015). In contrast, higher salinity waters have elevated chlorophyll and O_2
408 concentrations (often supersaturated) associated with net primary production and the
409 consumption of protons, typically occurring at the mouth of the Estuary and the margins of the
410 Bay (Voynova *et al.* 2015). In other salt marsh ecosystems, additional processes like CO_2
411 degassing and nitrification also play a large role in proton cycling, but the rates of these
412 processes remain uncharacterized in this system (Jiang *et al.* 2008, Hofmann *et al.* 2009).

413 The respiration of organic matter produces both TA and DIC, and directly impacts the
414 buffering capacity of natural waters (Wang & Cai 2004). As DIC approaches equality with TA,
415 buffering is reduced and waters are more susceptible to large changes in pH (Cai *et al*. 2001).
416 While mean $[H_T^+]$ were similar in the Spring (24.6 nmol kg^{-1} ± 0.2 S.E.) and Summer (22.8 nmol
417 kg^{-1} ± 0.2 S.E.), a sampling of TA and DIC over a Spring and Summer tidal cycle shows the
418 processes controlling proton cycling differ between the seasons (Fig. 6). The elevated
419 concentrations of TA and DIC during the Summer ebb tide, relative to the Spring, are consistent
420 with the export of both constituents from the surrounding salt marshes due to the respiration of
421 accumulated organic matter. Salt marshes surrounding the lower Murderkill are a sink for
422 organic matter and, as such, these marshes contribute both TA and DIC to the Estuary that vary
423 seasonally and affect the waters' buffering capacity (Wang & Cai 2004, Sharp 2011, Ullman *et*
424 *al.* 2013, Wang *et al.* 2016). The reactive organic matter that likely drives proton production and
425 cycling in the Murderkill River is a mixture of marine and freshwater (upper watershed
426 cyanobacterial blooms) phytoplankton, vascular plant detritus, and suspended sedimentary
427 particles (Ullman *et al.* 2013, Andres *et al.* 2019). Variations in these sources over time
428 ultimately influence net watershed respiration, and thus $[H_T^+]$, beyond that of non-tidal mean

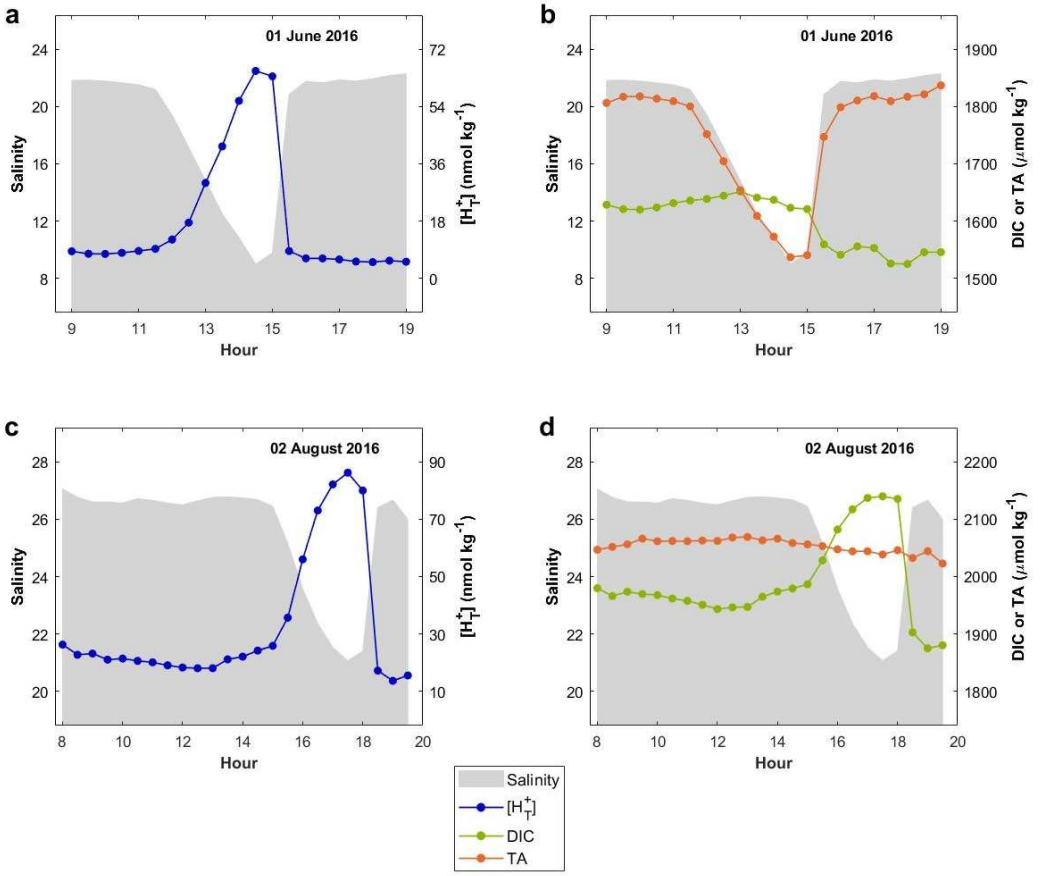

429

430 **Fig. 6.** Tidal dynamics of $[H_T^+]$ (blue, a & c), DIC (green, b & d) and TA (orange, b & d) with
431 respect to salinity (grey) for a Spring (a, b) and Summer (c, d) sampling of a full tidal cycle.
432 Discreet samples were taken half-hour for DIC and TA, while salinity and $[H_T^+]$ were measured
433 by the SeapHOx sensor at the same interval.

434

435 discharge alone (Voynova *et al.* 2015). More research is underway to better understand the
436 magnitude of organic matter respiration, along with other biogeochemical processes and
437 meteorological phenomenon, on proton production and transport within the Murderkill Estuary.

438 *3.4 Strengths and Limitations of the Proton Flux Method*

439 The proton flux method is not mutually exclusive of other, more established methods for
440 characterizing the acidification of estuaries and coastal waters. But rather, is another tool in the
441 toolbox to disentangle the complexities of acidification that include processes like the absorption
442 of anthropogenic carbon, net community production and calcification, and air-sea gas exchange,
443 among numerous other factors. The present methodology provides a novel way of using physical
444 forcing (discharge) to scale down from regional to local influences (and vice versa), assess the
445 magnitude of proton dynamics in smaller systems and resolve how these dynamics may buffer or
446 further acidify larger systems. The present case study clearly demonstrates that further
447 acidification or buffering can occur as a result of inter-system interactions and exchange within
448 the freshwater-influenced Delaware Bay-Murderkill Estuary system; dynamics that existing
449 methods for the study and modeling of estuarine and coastal ocean acidification may fail to
450 accurately estimate or include (Kwiatkowski & Orr 2018). Models are only as good as the data
451 that feeds them. If the models only capture constant and idealized variability in tidal signals and
452 exchange, then past approaches to the study of coastal and estuarine acidification may result in
453 substantial and/or disproportionate error in extrapolating from present to future acidification
454 trends and dynamics.

455 The proton flux method ultimately captures and integrates the real, *in situ* variability
456 representative of estuarine processes. In addition to the astronomical variability in tidal cycles
457 over time (e.g., neap vs. spring tides), the balance between freshwater discharge and tidal forcing

458 changes over time. The proton flux method allows researchers to integrate natural, asymmetric
459 variability into their methods and analyses. This variability affects the carbonate system by
460 altering rates of dilution and buffering capacity. Variability also influences calculated metrics
461 like the Revell Factor which describes the dynamic ability of the global oceans to absorb
462 atmospheric CO_2 and remains a key characteristic for estimating acidification based on the
463 oceanic uptake of anthropogenic carbon (Carter *et al*. 2019, Egleston *et al*. 2010). The method as
464 shown here incorporates both high temporal variability and, indirectly, spatial variability by
465 sampling the waters from two different end-members over the course of a tidal cycle.

466 The proton flux method provides advantages over other approaches, but it is not without
467 its limitations. The method reveals the net result of proton cycling and the upstream or
468 downstream proton sources and sinks, but it does not identify the specific processes (e.g.,
469 primary production or anaerobic respiration) that produce and consume protons. Additional
470 sampling of other parameters is needed to define and quantify the rates of these component
471 processes. Similarly, there is still a need to calibrate the pH sensors by measuring marine CO_2
472 system parameters (DIC and TA in this study) in the field, so the method is not exclusive of
473 other methods that examine acidification. Discharge measurements are also needed, which may
474 limit the use of this method in some locations. The mouth of the Murderkill Estuary is a well-
475 mixed system, so the data presented here represents the entire water column. Using the proton
476 flux method in stratified water columns would require additional resources, but is still feasible.
477 For example, additional monitoring that included depth profiling or the use of multiple sensors
478 could account for differential proton cycling occurring in the various, vertically stratified water
479 masses.

480

4. Conclusions and the Future of Proton Fluxes

The present work demonstrates the tidal and non-tidal dynamics of $[H_T^+]$ in an estuarine ecosystem. Using continuous, high frequency monitoring to track proton concentrations, together with discharge measurements, we can now precisely quantify the upstream and downstream fluxes of protons and the net direction of coastal acidification (i.e., sources vs. sinks). The Murderkill Estuary was used as a case study to demonstrate this novel way of characterizing acidification of coastal waters, and show temporal changes, from minutes to months, in the magnitude and direction of acidification. Together, a complementary approach that combines proton modeling and advanced time series analyses with measured concentrations using high-frequency autonomous sensors as model inputs and validation can provide a powerful technique to resolve current estuarine acidification mechanisms and trends (Hofmann *et al*. 2009, Fassbender *et al*. 2017, Feely *et al*. 2018, Kwiatkowski & Orr 2018, Miller *et al*. 2018, Pacella *et al*. 2018). With the appropriate sensors, similar monitoring and analyses can be performed in any free-flowing freshwater, estuarine or marine system and provides one more tool to identify those water bodies that are receiving elevated $[H_T^+]$, and may be more vulnerable to future acidification.

Proton concentration, or pH, is known as a "master" variable of aquatic biogeochemistry because it is both affected by and governs so many processes (Stumm & Morgan 1996). As such, proton cycling is a more appropriate way to view and quantify estuarine and coastal acidification (Hofmann *et al.* 2010, Fassbender *et al*. 2017, Kwiatkowski & Orr 2018). Proton concentrations are a more robust environmental indicator of acidification than pH because changes in pH are related not only to proton concentration, but also the initial pH of the water body and its temperature- and salinity-dependent buffer capacity (Fassbender *et al*. 2017). The present work

504 is meant to stimulate additional discussion already occurring in the literature on the way
505 researchers measure and characterize the acidification of natural waters by moving towards the
506 direct measurement, reporting and analysis of proton concentrations, in addition to pH and other
507 marine CO_2 system parameters (e.g., Hofmann *et al.* 2010, Fassbender *et al*. 2017, Kwiatkowski
508 & Orr 2018). The precise controls of proton production and consumption are not, as yet, known
509 for the Murderkill Estuary. However, the tools presented here will provide the basis for further
510 studies to improve our mechanistic understanding of the processes that drive proton production,
511 consumption, and transport within this and other systems and when used in conjunction with
512 other established methods will provide a better understanding of the sensitivity of estuaries to
513 current and future acidification.

514

515

516 **AUTHOR INFORMATION:**

517 **Corresponding Author**

518 *email: dpettay@uscb.edu

519 **Author Contributions**

520 The manuscript was written through contributions of all authors. All authors have given approval
521 to the final version of the manuscript.

522 **ACKNOWLEDGMENT:**

523 We thank the Kent County Board of Public Works (Diana Golt, Director, and Hans Medlarz, and
524 Andrew Jackubowitch, former directors), the Kent County Levy Court, the Watershed

525 Assessment Branch at the Delaware Department of Natural Resources and Environmental
526 Control (John Schneider and Hassan Mirsajadi), and US Geological Survey in (Anthony Tallman
527 and Betzaida Reyes in Dover, Delaware) for their financial, material, and technical support for
528 this project. Lillian Wong (Delaware Geological Survey) drafted Fig. 1.

529

530 **REFERENCES:**

531 Andres, A.S. (2004). Ground-water recharge potential mapping in Kent and Sussex Counties,
532 Delaware. Report of Investigations 66. Delaware Geological Survey, Newark, DE. 20
533 pgs.

534 Andres, A.S., C.R. Main, D.T. Pettay, and W.J. Ullman (2019). Hydrological controls of
535 cyanobacterial blooms in Coursey Pond, Delaware (USA). *Journal of Environmental*
536 *Quality* 48: 73-82.

537 Aufdenkampe, A. K., Mayorga, E., Raymond, P. A., Melack, J. M., Doney, S. C., Alin, S. A.,
538 Aalto, R. E., and Yoo, K. (2011). Riverine coupling of biogeochemical cycles between
539 land, oceans, and the atmosphere. *Frontiers in Ecology and the Environment, 9*(1): 53-60.

540 Bates, R. G. (1973). Determination of pH: Theory and Practice, 2ed. Wiley-Interscience.

541 Borges, A.V., and N. Gypens (2010). Carbonate chemistry in the coastal zone responds more
542 strongly to eutrophication than to ocean acidification, *Limnology and Oceanography*, 55:
543 346–353

544 Bresnahan Jr., P.J., T.R. Martz, Y. Takeshita, K.S. Johnson, and M. LaShomb (2014). Best
545 practices for autonomous measurement of seawater pH with the Honeywell Durafet.
546 *Methods in Oceanography*.

547 Butler, R. A., Covington, A.K., and Whitfield, M. (1985). The determination of pH in estuarine
548 waters. II: Practical considerations. *Oceanol. Acta,* 8(4): 433-39.

549 Cai, W.-J., Hu., X., Huang, W.-J., Jiang, L.-Q., Wang, Y., Peng, T.-H., and Zhang, X. (2010).
550 Alkalinity Distributions in the western North Atlantic Ocean margins. *Journal of*
551 *Geophysical Research: Oceans*, 115: 1-15.

552 Cai, W.-J., Hu, X., Huang, W.-J., Murrell, M.C., Lehrter, J.C., Lohrenz, S.E., Chou, W.-C., Zhai,
553 W., Hollibaugh, J.T., Wang, Y., Zhao, P., Guo, X., Gundersen, K., Dai M. and Gong, G.-
554 C. (2011). Acidification of subsurface coastal waters enhanced by eutrophication. *Nature*
555 *Geosciences*, 23: 766-770.

556 Cai, W.-J., and Wang, Y. (1998). The chemistry, fluxes, and sources of carbon dioxide in the
557 estuarine waters of the Satilla and Altamaha Rivers, Georgia. *Limnology and*
558 *Oceanography,* 43(4): 657-668.

559 Cai, W.-J., Wiebe, W.J., Wang Y., Sheldon J.E. (2000). Intertidal marsh as a source of dissolved
560 inorganic carbon and a sink of nitrate in the Satilla River-estuarine complex in the
561 southeastern U.S., *Limnology and Oceanography*, 8: 1743-1752.

562 Carstensen, J., and Duarte, C. M. (2019). Drivers of pH variability in coastal ecosystems.
563 *Environmental Science & Technology*, *53*(8): 4020-4029.

564 Carter, B. R., Feely, R. A., Wanninkhof, R., Kouketsu, S., Sonnerup, R. E., Pardo, P. C., Sabine,
565 C. L., Johnson, G. C., Sloyan, B. M., Murata, A. Mecking, S., Tilbrook, B., Speer, K.,
566 Talley, L. D., Millero, F. J., Wijffels, S. E., Macdonald, A. M., Gruber, N., and Bullister,
567 J. L. (2019). Pacific anthropogenic carbon between 1991 and 2017. *Global*
568 *Biogeochemical Cycles*, *33*(5): 597-617.

569 Chappell, N.A., Jones, T.D., Tych, W. (2017) Sampling frequency for water quality variables in
570 streams: Systems analysis to quantify minimum monitoring rates. *Water Research,* 123:
571 49-57.

572 Dickson, A.G. (1984). pH scales and proton-transfer reactions in saline media such as sea water.
573 *Geochimica et Cosmochimica Acta*. 48: 2299-2308.

574 Dickson, A.G. (1990). Standard potential of the reaction: AgCl (s) + 1/2 H_2 (g) = Ag (s) + HCl
575 (aq), and the standard acidity constant of the ion HSO^-_4 in synthetic sea water from
576 273.15 to 318.15 K. *Journal of Chemical Thermodynics*, 22 (2): 113-127.

577 Dickson, A.G. (1993). The measurement of seawater pH. *Marine Chemistry* 44:131-142.

578 DNREC 2006. Technical Analysis for the Proposed Murderkill River Bacteria TMDL, Delaware
579 Department of Natural Resources and Environmental Control, Dover. Pp 35.

580 Duarte, C.M., Hendriks, I.E., Moore, T.S., Olsen, Y.S., Steckbauer, A., Ramajo, L., Carstensen,
581 J., Trotter, J.A., and McCulloch, M. (2013). Is ocean acidification an open-ocean
582 syndrome? Understanding anthropogenic impacts on seawater pH. *Estuaries and Coasts,*
583 36: 221-236.

584 Dzwonkowski, B., Wong, K.C., Ullman, W.J. (2014). Water level and velocity characteristics of
585 a salt marsh channel in the Murderkill Estuary, Delaware. *Journal of Coastal Research,*
586 30: 63-74.

587 Easley, R. A., and Byrne, R. H. (2012). Spectrophotometric calibration of pH electrodes in
588 seawater using purified m-Cresol Purple. *Environental Science and Techology,* 46(9):
589 5018-5024.

590 Egleston, E. S., Sabine, C. L., and Morel, F. M. (2010). Revelle revisited: Buffer factors that
591 quantify the response of ocean chemistry to changes in DIC and alkalinity. *Global*
592 *Biogeochemical Cycles*, *24*(1).

593 Fassbender, A. J., Alin, S. R., Feely, R. A., Sutton, A. J., Newton, J., Krembs, C., *et al*. (2018a).
594 Seasonal carbonate chemistry variability in marine surface waters of the Pacific
595 Northwest. *Earth System Science Data* 10: 1367–1401. doi:
596 10.1371/journal.pone.0089619

597 Fassbender, A. J., Rodgers, K. B., Palevsky, H. I., & Sabine, C. L. (2018b). Seasonal asymmetry
598 in the evolution of surface ocean pCO_2 and pH thermodynamic drivers and the influence
599 on sea-air CO2 flux. *Global Biogeochemical Cycles*, 32: 1476–1497.

600 Fassbender, A. J., Sabine, C. L., & Palevsky, H. I. (2017). Nonuniform ocean acidification and
601 attenuation of the ocean carbon sink. *Geophysical Research Letters*, *44*(16): 8404-8413.

602 Feely, R.A. Alin, S.R, Newton, J., Sabine, C.L., Warner, M., Devol, A., Krembs, C., Maloy, C.
603 (2010). The combined effects of ocean acidification, mixing, and respiration on pH and
604 carbonate saturation in an urbanized estuary. *Estuarine Coastal & Shelf Science* 88: 442–
605 449.

606 Ganju, N.K., Schoellhamer, D.H., and Bergamaschi, B.A. (2005). Suspended sediment fluxes in
607 a tidal wetland: measurement, controlling factors, and error analysis. *Estuaries* 28: 812-
608 822.

609 Gonski, S.F., W.-J.Cai, W.J. Ullman, A. Joesoef, C.R. Main, D. T. Pettay, and T.R. Martz
610 (2018). Assessment of the suitability of Durafet-based sensors for pH measurement in
611 dynamic estuarine environments. *Estuarine, Coastal and Shelf Science*. 200: 152-168.

612 Gran, G. (1950). Determination of the equivalence point in potentiometric titrations. *Acta*
613 *Chemica Scandinavica,* 4: 559-577.

614 Gran, G. (1952). Determination of the equivalence point in potentiometric titrations–Part II. *The*
615 *Analyst,* 77(920): 661-671.

616 Hofmann, A.F., Meysman, F.J.R., Soetaert, K. and Middelburg, J.J. (2008). A step-by-step
617 procedure for pH model construction in aquatic systems. *Biogeosciences* 5: 227-251.

618 Hofmann, A.F., Middelburg, J.J., Soetaert, K. and Meysman, F.J.R. (2009). pH modelling in
619 aquatic systems with time-variable acid-base dissociation constants applied to the turbid,
620 tidal Scheldt estuary. *Biogeosciences* 6: 1539-1561.

621 Hofmann, A.F., J.J. Middelburg, K. Soetaert, D.A. Wolf-Gladrow, and F.J.R. Meysman (2010).
622 Proton Cycling, buffering, and reaction stoichiometry in natural waters. *Marine*
623 *Chemistry*, 121: 246-255.

624 Hofmann, G.E., Smith, J.E., Johnson, K.S., Send, U., Levin, L.A., Micheli, F., Paytan, A., Price,
625 N.N., Peterson, B., Takeshita, Y., Matson, P.G., Derse-Crook, E., Kroeker, K.J., Gambi,
626 M., Rivest, E. B., Frieder, C.A., Yu, P.C., and Martz, T.R. (2011). High-frequency
627 dynamics of ocean pH: a multi-ecosystem comparison. *PLoS One*, 6*(12)*.

628 Huang, W.-J., Wang, Y., and Cai, W.-J. (2012). Assessment of sample storage techniques for
629 total alkalinity and dissolved inorganic carbon in seawater. *Limnology and*
630 *Oceanography: Methods,* 10(9): 711-717.

631 Joesoef, A., Kirchman, D. L., Sommerfield, C. K. and Cai, W.-J. (2017). Seasonal variability of
632 the inorganic carbon system in a large coastal plain estuary. *Biogeosciences* 14: 4949-
633 4963.

634 Jokiel, P.L. (2016). Predicting the impact of ocean acidification on coral reefs: evaluating the
635 assumptions involved. Journal of Marine Science 73(3): 550–557.

636 Kline DI, Teneva L, Hauri C, Schneider K, Miard T, Chai A, et al. (2015). Six Month In Situ
637 High-Resolution Carbonate Chemistry and Temperature Study on a Coral Reef Flat
638 Reveals Asynchronous pH and Temperature Anomalies. *PLoS ONE* 10(6): e0127648.

639 Kwiatkowski, L., & Orr, J. C. (2018). Diverging seasonal extremes for ocean acidification during
640 the twenty-first century. *Nature Climate Change*, *8*(2): 141.

641 Lee, K., Kim, T.-W., Byrne, R. H., Millero, F. J., Feely, R. A., and Liu, Y.-M. (2010). The
642 universal ratio of boron to chlorinity for the North Pacific and North Atlantic oceans.
643 *Geochimica et Cosmochimica Acta, 74*(6): 1801-1811.

644 Ligges, U., et al. (2013). signal: Signal processing. URL: http://r-forge.r-
645 project.org/projects/signal/.

646 Martz, T.R., J. G Connery, K.S. Johnson (2010). Testing the Honeywell Durafet® for seawater
647 pH applications. *Limnology and Oceanography Methods* 8:172-184.

648 Millero, F. J., Graham, T. B., Huang, F., Bustos-Serrano, H., and Pierrot, D. (2006). Dissociation
649 constants of carbonic acid in seawater as a function of salinity and temperature. *Marine*
650 *Chemistry*, *100*(1): 80-94.

651 Miller, C.A., Pocock, K., Evans, W., and Kelley, K.L. (2018). An evaluation of the performance
652 of Sea-Bird Scientific's SeaFET autonomous pH sensor: Considerations for the broader
653 oceanographic community. *Ocean Science,* 14: 751-768.

654 Martz, T.R., Daly, K.L., Byrne, R.H., Stillman, J.H., and Turk, D. (2015). Technology for ocean
655 acidification research: Needs and availability. *Oceanography, 28*(2): 40-47.

656 Newton, J. A., Feely, R. A., Jewett, E. B., Williamson, P., and Mathis, J. (2015). Global Ocean
657 Acidification Observing Network: Requirement and Governance Plan. 2nd ed., *GOA-ON*.

658 Pierrot, D., Lewis, E., and Wallace, D. W. R. (2006). CO2SYS DOS Program Developed for
659 CO_2 System Calculations. *ORNL/CDIAC-105, Carbon Dioxide Information Analysis*
660 *Center, Oak Ridge National Laboratory, US Department of Energy, Oak Ridge, TN.*

661 Provoost, P., Van Heuven, S., Soetaert, K., Laane, R. W. P. M., and Middelburg, J. J. (2010).
662 Seasonal and long-term changes in pH in the Dutch coastal zone. *Biogeosciences*, *7*(11):
663 3869.

664 Rivest EB, Gouhier TC (2015). Complex Environmental Forcing across the Biogeographical
665 Range of Coral Populations. *PLoS ONE* 10(3): e0121742.

666 Sharp, J.H. (2011). Primary Production in the Murderkill River. A Report to Kent County and
667 Delaware DNREC. Unpublished Report:
668 http://www.dnrec.delaware.gov/swc/wa/Documents/WAS/Murderkill%20River%20Repo
669 rts/New%20Murderkill%20Page/1.%20%20Primary%20Production%20Study%20Report
670 .pdf

671 Skeffington, R.A., Halliday, S.J., Wade, A.J., Bowes, M.J., and Loewenthal, M. (2015) Using
672 high-frequency water quality data to assess sampling strategies for the EU Water
673 Framework Directive. *Hydrology and Earth Systems Science*, 19: 2491–2504.

674 Stumm, W., Morgan, J.J. (1996) Aquatic Chemistry: Chemical Equilibria and Rates in Natural
675 Waters, third ed. Wiley-Interscience.

676 Sunda, W.G. and W.J. Cai, (2012). Eutrophication induced CO2 –Acidification of subsurface
677 coastal waters: Interactive effects of temperature, Salinity, and pCO_2. *Environmental*
678 *Science and Technology* 46:10651-10659.

679 Takeshita, Y., Frieder, C. A., Martz, T. R., Ballard, J. R., Feely, R. A., Kram, S., Nam, S.,
680 Navarro, M. O., Price, N. N. and Smith, J. E. (2015). Including high-frequency variability
681 in coastal ocean acidification projections. *Biogeosciences* 12: 5853-5870.

682 Takeshita, Y., Martz, T. R., Johnson, K. S., and Dickson, A. G. (2014). Characterization of an
683 Ion-Selective Field Effect Transistor and Chloride Ion-Selective Electrodes for pH
684 Measurements in Seawater. *Analytical Chemistry,* 86 (22): 1189-1195.

685 Ullman, W.J., Aufdenkampe, A., Hays, R.L., Dix, S. (2013). Nutrient Exchange between a Salt
686 Marsh and the Murderkill Estuary, Kent County, Delaware. Part C. Technical Report.
687 Delaware Department of Natural Resources and Environmental Control, Dover, DE
688 Unpublished Report.
689 http://www.dnrec.delaware.gov/swc/wa/Documents/WAS/Murderkill%20River%20Repo
690 rts/New%20Murderkill%20Page/3.%20Study%20of%20Tidal%20Marsh%20Fluxes%20
691 of%20Nutrients%20and%20DO.pdf

692 Velinsky, D., C. Sommerfield, D. Charles (2010). Vertical Profiles of Radioisotopes, Nutrients,
693 and Diatoms in Sediment Cores from the Tidal Murderkill River Basin: A Historical
694 Analysis of Ecological Change and Sediment Acrretion. (PCER Report 10-01).
695 http://www.dnrec.delaware.gov/Admin/DelawareWetlands/Documents/Data%20Portal/A
696 NSP%20Murderkill%20River%20Final%20Report%20see%20email%20from%20Chris
697 %20B%20relating.pdf

698 Voynova, Y.G., Lebaron, K. C., Barnes, R.T., and Ullman, W.J. (2015). *In situ* response of bay
699 productivity to nutrient loading from a small tributary: The Delaware Bay-Murderkill
700 Estuary tidally-coupled biogeochemical reactor. *Estuarine, Coastal, and Shelf Science,*
701 160: 33-48.

702 Voynova, Y.G., Sharp, J.H., 2012. Anomalous biogeochemical response to a flooding event in
703 the Delaware Estuary: a possible typology shift due to climate change. *Estuaries Coasts*
704 35: 943e958.

705 Wallace, R.B., Baumann, H., Grear, J.S., Aller, R.C., Gobler, C.J. (2014). Coastal Ocean
706 Acidification: the other eutrophication problem. Estuarine. Coastal and. Shelf Science.
707 148:1-13.

708 Wang, Z.A. & Cai, W.-J. (2004). Carbon dioxide degassing and inorganic carbon export from a
709 marsh-dominated estuary (the Duplin River): A marsh CO_2 pump. *Limnology and*
710 *Oceanography* 49: 314-354.

711 Wang, Z. A., Kroeger, K. D., Ganju, N. K., Gonneea, M. E., Chu, S. N. (2016). Intertidal salt
712 marshes as an important source of inorganic carbon to the coastal ocean. *Limnology and*
713 *Oceanography* 61: 1916-1931.

714 Whitfield, M., Bulter, R. A., and Covington, A. K. (1985). The determination of pH in estuarine
715 waters. I: Definitions of pH scales and selection of buffers. *Oceanol. Acta, 8*(4): 423-432.

716 Wong, K.-C., Dzwonkowski, B., Ullman, W.J. (2009). Temporal and spatial variability of sea
717 level and volume flux in the Murderkill Estuary. *Estuarine, Coastal and Shelf Science*,
718 84: 440-446.

719 Wootton, J. T., and Pfister, C. A. (2012). Carbon system measurements and potential climatic
720 drivers at a site of rapidly declining ocean pH. *PLoS One, 7*(12): e53396.

721

722

723

724

725